ARTICULAR CARTILAGE MECHANICAL AND BIOCHEMICAL PROPERTY RELATIONS BEFORE AND AFTER IN VITRO GROWTH

Timothy Ficklin*, Gregory Thomas*, James C. Barthel*, Anna Asanbaeva[†], Eugene J. Thonar[#+], Koichi Masuda[#], Albert C. Chen[†], Robert L. Sah[†], Andrew Davol*, Stephen M. Klisch*

*Department of Mechanical Engineering
California Polytechnic State University, San Luis Obispo, CA

[†]Department of Bioengineering,
University of California-San Diego, La Jolla, CA

[#]Departments of Biochemistry and Orthopedic Surgery
Rush University Medical Center, Chicago, IL

[+]Department of Internal Medicine
Rush University Medical Center, Chicago, IL

PUBLISHED CITATION

Ficklin T, Thomas G, Barthel JC, Thonar EJ, Masuda K, Asanbaeva A, Chen AC, Sah RL, Davol A, Klisch SM. Articular cartilage mechanical and biochemical property relations before and after in vitro growth. *Journal of Biomechanics*, 40:3607-3614, 2007.

Keywords: cartilage, growth, collagen, crosslinks, biomechanics.

Address all correspondence to:
Stephen M. Klisch, Ph.D.
Associate Professor
Mechanical Engineering Department
California Polytechnic State University
San Luis Obispo, CA 93407
(805) 756-1308; FAX (805) 756-1137
sklisch@calpoly.edu

ABSTRACT

The aim of this study was to design *in vitro* growth protocols that can comprehensively quantify articular cartilage structure-function relations via measurement of mechanical and biochemical properties. Newborn bovine patellofemoral groove articular cartilage explants were tested sequentially in confined compression (CC), unconfined compression (UCC), and torsional shear before (D0 i.e. day zero) and after (D14 i.e. day 14) unstimulated *in vitro* growth. The contents of collagen (COL), collagen-specific pyridinoline (PYR) crosslinks, glycosaminoglycan, and DNA significantly decreased during *in vitro* growth; consequently, a wide range of biochemical properties existed for investigating structure-function relations when pooling the D0 and D14 groups. All D0 mechanical properties were independent of compression strain while only Poisson's ratios were dependent on direction (i.e. anisotropic). Select D0 and D14 group mechanical properties were correlated with biochemical measures; including (but not limited to) results that CC/UCC moduli and UCC Poisson's ratios were correlated with COL and PYR. COL network weakening during *in vitro* growth due to reduced COL and PYR was accompanied by reduced CC/UCC moduli and increased UCC Poisson's ratios.

INTRODUCTION

Articular cartilage (AC) contains cells (i.e. chondrocytes) embedded in a matrix containing glycosaminoglycans (GAGs), collagens (COLs), and water. GAGs, which form larger proteoglycan (PG) molecules, have fixed negative charges that generate a swelling pressure that is restrained by the crosslinked COL network (CN) (Venn and Maroudas, 1977). The microstructural properties of the GAGs and the CN are thought to be predominantly responsible for the tissue's biomechanical properties, commonly characterized as anisotropic (i.e. dependent

on direction), asymmetric (i.e. different in tension and compression), and nonlinear (i.e. dependent on strain) (Woo et al., 1979; Soltz and Ateshian, 2000; Klisch, 2007).

Continuum mechanics cartilage growth mixture (CGM) models have been developed that allow AC to be modeled as a mixture of constituents that can grow at different rates (Klisch et al., 2003; Davol et al., 2007). These models include many adjustable parameters; in order to not over-parameterize a growth simulation, comprehensive mechanical and biochemical property data are needed. However, *in vitro* growth studies are limited with respect to the breadth of measured mechanical properties; for example, a recent validation analysis of a CGM model was limited to predicting tensile modulus at 20% strain (Klisch et al., 2007a).

Motivated by the need for comprehensive data in order to develop accurate CGM models, the aim of this study was to design *in vitro* growth protocols that can comprehensively quantify AC structure–function relations. Mechanical properties of explants harvested in different directions were measured before growth in confined compression (CC), unconfined compression (UCC), and torsional shear (TS). Other explants were grown *in vitro* to provide baseline growth laws (i.e. the rate of mass deposition per unit current mass) under unstimulated conditions in order to quantify the effect of mechanical loading on the growth laws in future studies. Novel features of the protocols included the simultaneous measurement of two orthogonal UCC Poisson's ratios (i.e. the negative ratio of lateral expansion strain to applied compression strain) in contrast to previous optical measurements of one Poisson's ratio at a time (Jurvelin et al., 1997; Wong et al., 2000; Laasanen et al., 2003; Wang et al., 2003; Kiviranta et al., 2006) and comprehensive

mechanical property correlations with biochemical properties including COL specific pyridinoline (PYR) crosslinks.

The specific aims were to: (1) design experimental protocols to measure direction- and strain-dependent AC mechanical properties; (2) measure mechanical and biochemical properties before and after *in vitro* growth; and (3) investigate structure-function relations between mechanical and biochemical properties.

METHODS

Sample Preparation

Full-thickness blocks (n=19) of newborn (~1-3 week old) bovine AC were harvested from the medial ridge of the patellofemoral groove (PFG) of 19 unpaired knees (Fig. 1). Eleven blocks were used for testing before *in vitro* growth (D0 i.e. day zero). Each block was sliced to produce three orthogonal slices: a medial-lateral (ML-D0) slice normal to the ML direction and ~ parallel to the local split-line direction (Williamson et al., 2003a), an anterior-posterior (AP-D0) slice normal to the AP direction, and an axial (AX-D0) slice parallel to the articular surface at a mean depth of 2 mm. In preliminary tests the AP-D0 and ML-D0 groups exhibited similar mechanical properties; consequently, AP-D0 slices were used only for biochemical testing. Each slice was planed to 1mm height (h) using a freezing stage mounted on a sledge microtome. Cylindrical discs (diameter d = 3.2 mm, h = 1 mm) were punched from each slice so that the center of each disc was ~ 2 mm from the surface. A trypan blue dye line on one disc surface was used to track anatomic direction. The discs were frozen at -20 C and thawed at room temperature before testing.

The remaining 8 blocks were used for mechanical and biochemical testing after *in vitro* growth (D14 i.e. day 14). Each block was used to obtain one axial (AX-D14) slice (~10 x 6 x .7 mm) parallel to the surface at a mean depth of 2 mm. The slices were incubated in medium (DMEM supplemented with 20% FBS and 100 μg/ml ascorbate) for 14 days using existing protocols (Asanbaeva et al., 2007a). After 14 days the WW was measured and the slices were frozen at -20 C. Prior to mechanical testing, the slices were thawed at room temperature and punched into cylindrical discs (d = 4.8 mm, h = 0.7 mm). The diameter, height, and WW of the discs were measured before each mechanical experiment.

Mechanical Testing

All mechanical tests were performed in test medium consisting of PBS (0.15M NaCl at pH 7.1 plus buffers) and proteinase inhibitors. ML-D0 and AX-D0 specimens were tested in sequential CC (n=10), UCC (n=11), and TS (n=7) experiments while AX-D14 specimens were tested in sequential CC (n=8) and UCC (n=8) experiments. The CC experiments were performed according to established protocols (Chen et al., 2001a; Williamson et al., 2001) in a materials testing machine (Enduratec ELF 3200). Specimens were loaded in sequential 400 sec. ramps to 15, 30, and 45% strains while allowing for stress relaxation to equilibrium determined using a termination criterion of a change in stress less than 0.003MPa over 180 sec. The mechanical properties of the first three AX-D14 specimens were considerably degraded such that compressive loading to 45% strain caused irreversible damage; subsequent tests with AX-D14 specimens were limited to 15 and 30% compressive strains. A series of oscillatory displacements of 0.1 - 0.3% amplitude were superimposed on all three compressed equilibrium

states. From the equilibrium data, a CC secant modulus (i.e., total stress divided by total strain) H_A was calculated. From the dynamic data, the permeability constants k_0 and M were calculated (Chen et al., 2001a) using the strain dependent permeability function $k = k_0 e^{M\varepsilon}$ (Lai et al., 1981), where the strain $\varepsilon = \lambda - 1$ and the stretch λ (<1 for compression) in the compressed equilibrium state equals the ratio of the compressed to initial thicknesses.

New protocols were developed to perform the UCC experiments and TS experiments in the same test chamber (Fig. 2) in a materials testing machine (Dynastat). In UCC, impermeable platens were used to compress each specimen to 15, 30, and 45% strains using loading protocols similar to those for CC. A novel optical system was designed consisting of a light source, partially submerged right-angle prisms, a flat mirror, and a digital SLR camera. The optical system projected two perpendicular, lateral views of the disc to the camera simultaneously (Fig. 2A). Images were obtained after stress relaxation at each strain level and processed in MATLAB (Fig. 3) to calculate the lateral expansion of the disc in two directions. Two orthogonal UCC Poisson's ratios ν_{ij} (i=direction of applied loading, j=transverse strain component) and a secant UCC modulus E were calculated at each strain level. Upon completion of the UCC tests, platens were switched to porous platens and a 10% offset equilibrium compression strain was applied to perform the TS test (Fig. 2B). First, four cycles were applied from 0 to +0.5% shear strain, where each cycle consisted of ramping to +0.5% shear strain, allowing for stress relaxation to equilibrium (90 sec.), and unloading to 0. Then, four cycles were applied from 0 to -0.5% shear strain in a similar manner. In order to obtain repeatable results, the data from the first cycles to ±0.5% were discarded and the remaining data were used to calculate an equilibrium shear modulus μ (i.e. shear stress divided by engineering shear strain). These protocols resulted from

pilot tests so that there was no evidence in the data of slip at the specimen-porous platen interface during torsion while allowing for slip at the specimen-impermeable platen surface during UCC.

Biochemical Analysis

Biochemical properties were measured according to established protocols (Asanbaeva et al., 2007a). Biochemical properties were measured for the AX-D0 and ML-D0 groups using the adjacent AP-D0 slices, and measured directly from the mechanically tested AX-D14 specimens. The specimens were lyophilized, weighed dry, and digested using Proteinase K. The digest was analyzed to quantify DNA (McGowan et al., 2002), GAG (Farndale et al., 1986), hydroxyproline (Woessner, 1961), and PYR (Uebelhart et al., 1993). DNA was converted to cell number using a conversion factor of 7.7 pg DNA/cell (Kim et al., 1988). Hydroxyproline was converted to COL using a mass ratio of 7.25 COL/hydroxyproline (Herbage et al., 1977).

Statistical Analysis

For the D0 mechanical properties H_A, E, and ν_{ij} the effects of direction (ML vs. AX) and strain (15, 30, 45%) factors were investigated using two-way ANOVA (Excel) and post-hoc Tukey tests (custom MATLAB code). For the D0 mechanical properties k_0, M, and μ the effects of direction were investigated using t-tests. For biochemical composition the effects of growth were investigated using t-tests with the AX-D14 specimens and the AP-D0 specimens that were paired with the AX-D0 and ML-D0 specimens. For mechanical properties the effects of growth were investigated using t-tests with the AX-D0 and AX-D14 specimens. Correlations between mechanical and biochemical properties were investigated with two different linear regressions,

one that included both D0 and D14 specimens (i.e. AX-D0, ML-D0, AX-D14) and one that included only D0 specimens (i.e. AX-D0, ML-D0), and significances were assessed using t-test analysis of the regression slopes (custom MATLAB code). P values less than 0.05 were considered significant.

RESULTS

From the tests on AX-D0 and ML-D0 groups, CC modulus H_A and UCC modulus E did not depend on direction or strain level (Table 1, Fig. 4). However, a stress-softening trend (not significant) was observed as modulus was lowest at the 30% strain level for 9/10 CC specimens and 11/11 UCC specimens. The UCC Poisson's ratio ν_{13} was greater than the other Poisson's ratios at all strain levels (Table 1); ν_{13} was significantly greater than ν_{32} at 30 ($p<0.01$; Fig. 5) and 45% strains ($p<0.01$) but not at 15% strain ($p=0.11$) while the trend of ν_{13} greater than ν_{12} and ν_{31} was not significant at any strain level. The shear modulus μ was independent of direction (Table 1). A positive linear correlation ($p<0.05$) existed between μ and offset compression stress when pooling ML-D0 and AX-D0 specimens (Fig. 6), and the regression y-intercept value of 0.113 MPa suggests a value for the infinitesimal shear modulus.

From the tests on AX-D0, AP-D0, and AX-D14 groups, there were significant differences found in mechanical and biochemical properties before and after *in vitro* growth (Tables 1-2). H_A ($p<0.001$) and E ($p<0.001$) decreased and the Poisson's ratios ν_{31} ($p<0.01$) and ν_{32} ($p<0.01$) increased at both strain levels, but the permeability constants k_0 and M did not change (Table 1). The contents of COL ($p<0.001$), GAG ($p<0.05$), DNA ($p<0.001$), and PYR ($p<0.001$) decreased due to growth (Table 2).

Mechanical properties pooled from the ML-D0, AX-D0, and AX-D14 groups were correlated with biochemical contents (Figs. 7-8). COL was correlated with H_A ($p<0.01$), E ($p<0.0001$), ν_{31} ($p<0.05$), and ν_{32} ($p<0.05$) at 15, 30 (Fig. 7), and 45% strains, and with k_0 ($p<0.01$) and μ ($p<0.01$) (Fig. 7). PYR was correlated with H_A ($p<0.01$), E ($p<0.01$), ν_{31} ($p<0.05$), and ν_{32} ($p<0.05$) at 15, 30 (Fig. 7), and 45% strains. GAG was correlated with H_A ($p<0.05$) at 30 (Fig. 8) and 45% strains, with E ($p<0.001$) at 15, 30 (Fig. 8), and 45% strains. DNA was correlated with H_A ($p<0.01$) at 15 and 30% (Fig. 8) strains, with E ($p<0.05$) at 15, 30 (Fig. 8), and 45% strains, with ν_{31} ($p<0.05$) at 15% strain, with ν_{32} ($p<0.05$) at 30% (Fig. 8) strain, and with k_0 ($p<0.05$) (Fig. 8). Water content was correlated with k_0 ($p<0.01$) and with μ ($p<0.01$).

Without the inclusion of data after *in vitro* growth, the correlations were generally weaker (not shown). COL was correlated with H_A ($p<0.05$) at 30 and 45% strains, with E ($p<0.0001$) at 15, 30, and 45% strains, with ν_{12} ($p<0.05$) at 30% strain, with ν_{13} ($p<0.05$) at 15 and 30% strains, with ν_{31} ($p<0.05$) at 15, 30, and 45% strains, with ν_{32} ($p<0.05$) at 45% strain, and with μ ($p<0.001$). PYR was correlated with ν_{12} ($p<0.05$) at 15% strain and with M ($p<0.05$). GAG was not correlated with any of the D0 mechanical properties. DNA was correlated with ν_{12} ($p<0.05$) at 30% strain and with ν_{32} ($p<0.05$) at 15% strain. Water content was correlated with H_A ($p<0.05$) at 30 and 45% strains, with E ($p<0.05$) at 15, 30, and 45% strains, and with μ ($p<0.01$).

DISCUSSION

This study provides novel structure-function relations between mechanical and biochemical properties before and after *in vitro* growth. All D0 mechanical properties were independent of

compressive strain while only Poisson's ratios were dependent on direction (i.e., anisotropic). Since growth in FBS leads to an immature state evidenced by lower GAG, COL, and PYR, the protocol produced a wide range of biochemical content for investigating structure-function relations when pooling the D0 and D14 specimens. Select mechanical properties were correlated with biochemical measures; generally, correlations with the CN properties COL and PYR were strongest.

Although some studies suggest that compressive properties are best correlated with GAG (Mow and Ratcliffe, 1997), the result here that CC modulus is better correlated with COL does agree with several previous studies. For a more superficial region of bovine PFG AC, CC modulus was correlated with COL and GAG with R^2 values of 0.36 and 0.24, respectively (Williamson et al., 2001). One hypothesis offered in (Williamson et al., 2001) to explain the dependence of CC modulus on COL is that a higher COL content leads to a decrease in extrafibrillar volume where the GAGs reside and, consequently, to a higher effective fixed charge density which controls compressive properties (Basser et al., 1998). Also, other experimental studies using different protocols have suggested that the CN may provide compressive resistance in confined compression (Khalsa and Eisenberg, 1997; Chen et al., 2001b).

Previously, tension modulus has been shown to be significantly correlated with PYR (Williamson et al., 2003a); here, CC and UCC modulus and UCC Poisson's ratio were also correlated with PYR. Also, both CC and UCC moduli decreased by ~1 order of magnitude during growth as COL and PYR decreased; these results can be partly explained by CN weakening as evidenced by reductions in COL and PYR. These results are consistent with

reductions in tension modulus during unstimulated growth for specimens from the same tissue site (Williamson et al., 2003b; Asanbaeva et al., 2007b).

UCC Poisson's ratios were mostly dependent on the CN properties COL and PYR, as compared to GAG, DNA, and water. The UCC Poisson's ratios ν_{31} and ν_{32} increased ~3 times during growth, consistent with recent theoretical predictions that a weakened CN leads to increased UCC Poisson's ratios. For specimens harvested from the same site but a more superficial region (Asanbaeva et al., 2004), a continuum mechanics CGM model with COL remodeling predicted Poisson's ratios ν_{31} and ν_{32} to increase from 0.16 to 0.20 while PYR decreased from 137 to 89 nmol/g (Klisch et al., 2007a). Here, the increases in ν_{31} and ν_{32} were greater while PYR contents were lower (decreasing from 96 to 46 nmol/g). Although these absolute numbers are different, the trend of increasing Poisson's ratios with decreasing PYR is consistent among these studies.

Only Poisson's ratios were anisotropic as ν_{13} was greater than ν_{12} and ν_{31} and significantly greater than ν_{32}. The dependence of Poisson's ratios on CN properties offers an explanation for why ν_{13} is the largest Poisson's ratio. If the CN tensile stiffness is weakest in the 3-direction (i.e. normal to the surface), then for an applied UCC strain in the 1-direction the transverse strain in the 3-direction (ν_{13}) should be greater than that in the 2-direction (ν_{12}), as measured here and predicted by a nonlinear PG-COL stress balance model (Klisch et al., 2007b). The conclusion that Poisson's ratios depend mostly on CN properties strengthens a similar conclusion of (Kiviranta et al., 2006), whom reported a lower correlation (R^2=0.35) between Poisson's ratio and COL while not considering PYR content nor anisotropy.

Measured mechanical properties generally agreed with other studies with calf AC. CC moduli were similar to values for calf humeral head AC (0.64 MPa) (Soltz and Ateshian, 2000) and a more superficial layer of calf PGF AC (0.43) (Williamson et al., 2001). UCC moduli were similar to values for calf humeral head AC (0.60 MPa) (Soltz and Ateshian, 2000). UCC Poisson's ratios ν_{31} and ν_{32} were similar to values for calf humeral head AC (0.11) (Wong et al., 2000), bovine PFG AC (~0.20) (Laasanen et al., 2003), and middle zone calf glenohumeral AC (0.21-0.22) (Wang et al., 2003) while the observed anisotropy of Poisson's ratios agree with results for middle zone calf glenohumeral AC (Wang et al., 2003). The predicted infinitesimal modulus (0.11 MPa) was lower than a range of published values from other tissue sites (Mow and Ratcliffe, 1997), but similar to a value for calf humeral head AC (0.17 MPa) (Soltz and Ateshian, 2000) and adult bovine knee AC (0.14 MPa) (Khalsa and Eisenberg, 1997).

Stress softening in 19/20 compression specimens was observed, i.e. CC and UCC moduli were lowest at the 30% strain level. This trend, although not significant, agrees with results for calf glenohumeral AC (Chahine et al., 2004) and theoretical predictions by a linear triphasic model (Chahine et al., 2004) and a nonlinear PG-COL stress balance model (Klisch et al., 2006). In the latter nonlinear PG-COL stress balance model, the CN behaves as a highly nonlinear elastic material in tension that, in an unloaded configuration for a tissue specimen, supports a tensile pre-stress that restrains the swelling tendency of the PGs. As a consequence of this modeling assumption, a nonlinear UCC response is predicted as both modulus and Poisson's ratios drop substantially during the initial stages of UCC due to a decrease/increase in COL fiber tension in the loading/lateral directions, respectively (Klisch et al., 2007b). These predictions are supported by our observed decrease in UCC secant modulus from 15-30% strains but not by our observed

strain-independent Poisson's ratios; presumably the use of smaller strain increments would more effectively capture these nonlinear effects.

Limitations of the present study include a limited amount of mechanical tests following growth; tests were limited to 15 and 30% CC and UCC strains because preliminary tests resulted in weak grown specimens that were irreversibly damaged when loaded in CC or UCC to 45% strain. Grown specimens included only AX oriented specimens; this choice was made because the protocol regarding tissue size may have resulted in the growth of initially nonhomogeneous specimens if ML or AP slices were used. The possibility of nonhomogeneous properties is also a concern for the ML-D0 and AP-D0 groups. However, averaged biochemical measures for the AP-D0 and ML-D0 groups can be expected to be similar to values of smaller specimens at a mean depth of 2 mm as pilot biochemistry tests showed that contents did not vary between paired AX and ML specimens (n=8; p=0.72 and 0.98 for GAG and COL, respectively). Middle zone AC was harvested from immature animals as it was assumed that mechanical properties would be less anisotropic than AC from a more superficial region and/or from mature animals; consequently, the results from this and ongoing studies may be used to accomplish the long-term aim of quantifying the development of anisotropic structure-function properties during growth. COL, GAG, DNA, and PYR contents were all significantly different between the D0 and D14 groups; thus, it is not possible to attribute mechanical property changes to a decrease in any one component. This observation suggests the importance of analyzing these results with continuum mechanics models of growth, as described below, that can further quantify how the complex biochemical changes that occur during growth collectively affect mechanical properties.

This study provides structure-function data for a baseline growth protocol; future studies will be able to use these results to conduct validation analyses of CGM models while incorporating data from other protocols designed to enhance biomechanical properties. If the growth models can be validated, it may be possible to predict biomechanical changes of graft or engineered tissue constructs during *in vitro* stimulation and, consequently, to address limitations of cartilage repair strategies. For example, difficulties associated with osteochondral grafts include lateral integration with surrounding tissue, transplantation from low to high weight-bearing sites, and mismatch between donor and repair site thicknesses (Hangody and Fules, 2003; Horas et al., 2003).

ACKNOWLEDGEMENTS

Funding received from NSF (RS, AD, SK), NIH (KM, ET, RS), HHMI (UCSD for RS), and ONR (Department of Navy) (SK).

REFERENCES

Asanbaeva, A., McGowan, K. B., Masuda, K., Klisch, S. M., Thonar, E. J.-M. A., Sah, R. L., 2004. Mechanisms of cartilage growth: alteration and function and composition in vitro by deposition of collagen and proteoglycan matrix components. Trans Orthop Res Soc 29, 554.

Asanbaeva, A., Masuda, K., Thonar, E. J.-M. A., Klisch, S. M., Sah, R. L., 2007a. Regulation of immature cartilage growth by IGF-I, TGF-alpha 1, BMP-7, and PDGF-AB: role of metabolic balance between fixed charge and collagen network. Biomech Model Mechanobiol (In Press).

Asanbaeva, A., Masuda, K., Thonar, E. J.-M. A., Klisch, S. M., Sah, R. L., 2007b. Mechanisms of cartilage growth: modulation of balance between proteoglycan and collagen in vitro using chondroitinase ABC. Arthritis Rheum 56, 188-98.

Basser, P. J., Schneiderman, R., Bank, R. A., Wachtel, E., Maroudas, A., 1998. Mechanical properties of the collagen network in human articular cartilage as measured by osmotic stress technique. Arch Biochem Biophys 351, 207-19.

Chahine, N. O., Wang, C. C., Hung, C. T., Ateshian, G. A., 2004. Anisotropic strain-dependent material properties of bovine articular cartilage in the transitional range from tension to compression. J Biomech 37, 1251-1261.

Chen, A. C., Bae, W. C., Schinagl, R. M., Sah, R. L., 2001a. Depth- and strain-dependent mechanical and electromechanical properties of full-thickness bovine articular cartilage in confined compression. J Biomech 34, 1-12.

Chen, S. S., Falcovitz, Y. H., Schneiderman, R., Maroudas, A., Sah, R. L., 2001b. Depth-dependent compressive properties of normal aged human femoral head articular cartilage: relationship to fixed charge density. Osteoarthritis Cartilage 9, 561-9.

Davol, A., Bingham, M. S., Sah, R. L., Klisch, S. M., 2007. A nonlinear finite element model of cartilage growth. Biomech Model Mechanobiol (In Press).

Farndale, R. W., Buttle, D. J., Barrett, A. J., 1986. Improved quantitation and discrimination of sulphated glycosaminoglycans by use of dimethylmethylene blue. Biochim Biophys Acta 883, 173-177.

Hangody, L., Fules, P., 2003. Autologous osteochondral mosaicplasty for the treatment of full-thickness defects of weight-bearing joints. Ten years of experimental and clinical experience. J Bone Joint Surg 85-A, Supplement 2, 25-32.

Herbage, D., Bouillet, J., Bernengo, J.-C., 1977. Biochemical and physicochemical characterization of pepsin-solubilized type-II collagen from bovine articular cartilage. Biochem J 161, 303-312.

Horas, U., Pelinkovic, D., Herr, G., Aigner, T., Schnettler, R., 2003. Autologous chondrocyte implantation and osteochondral cylinder transplantation in cartilage repair of the knee joint. A prospective, comparative trial. J Bone Joint Surg Am 85-A(2), 185-92.

Jurvelin, J. S., Buschmann, M. D., Hunziker, E. B., 1997. Optical and mechanical determination of Poisson's ratio of adult bovine humeral articular cartilage. J Biomech 30, 235-41.

Khalsa, P. S., Eisenberg, S. R., 1997. Compressive behavior of articular cartilage is not completely explained by proteoglycan osmotic pressure. J Biomech 30, 589-94.

Kim, Y. J., Sah, R. L. Y., Doong, J. Y. H., Grodzinsky, A. J., 1988. Fluorometric assay of DNA in cartilage explants using Hoechst 33258. Anal Biochem 174, 168-176.

Kiviranta, P., Rieppo, J., Korhonen, R. K., Julkunen, P., Toyras, J., Jurvelin, J. S., 2006. Collagen network primarily controls Poisson's ratio of bovine articular cartilage in compression. Journal of Orthopaedic Research 24, 690-699.

Klisch, S. M., Chen, S. S., Sah, R. L., Hoger, A., 2003. A growth mixture theory for cartilage with applications to growth-related experiments on cartilage explants. J Biomech Eng 125, 169-179.

Klisch, S. M., Sah, R. L., Davol, A., 2006. Bimodular-orthotropic-polyconvex strain energy functions for the collagen-proteoglycan solid matrix of articular cartilage. In ASME Summer Bioengineering Conference Proceedings. Amelia Island, FL.

Klisch, S. M., 2007. A bimodular polyconvex anisotropic strain energy function for articular cartilage. J Biomech Eng 129, 250-258.

Klisch, S. M., Asanbaeva, A., Oungoulian, S. R., Thonar, E. J., Masuda, K., Davol, A., Sah, R. L., 2007a. A cartilage growth mixture model with collagen remodeling: validation protocols. ASME Journal of Biomechanical Engineering (In Review).

Klisch, S. M., Asanbaeva, A., Oungoulian, S. R., Thonar, E. J., Masuda, K., Davol, A., Sah, R. L., 2007b. A cartilage growth mixture model with collagen remodeling: validation protocols. In ASME Summer Bioengineering Conference Proceedings, Keystone, CO.

Laasanen, M., Toyras, J., Korhonen, R., Rieppo, J., Saarakkala, S., Nieminen, M., Hirvonen, J., Jurvelin, J. S., 2003. Biomechanical properties of knee articular cartilage. Biorheology 40, 133-40.

Lai, W. M., Mow, V. C., Roth, V., 1981. Effects of nonlinear strain-dependent permeability and rate of compression on the stress behavior of articular cartilage. J Biomech Eng 103, 61-66.

McGowan, K. B., Kurtis, M. S., Lottman, L. M., Watson, D., Sah, R. L., 2002. Biochemical quantification of DNA in human articular and septal cartilage using PicoGreen and Hoechst 33258. Osteoarthritis Cartilage 10(7), 580-7.

Mow, V. C., Ratcliffe, A., 1997. Structure and function of articular cartilage and meniscus. In: Mow, V. C., Hayes, W. C. (Eds.), Basic Orthopaedic Biomechanics. Raven Press, New York, pp. 113-178.

Soltz, M. A., Ateshian, G. A., 2000. A conewise linear elasticity mixture model for the analysis of tension-compression nonlinearity in articular cartilage. J Biomech Eng 122, 576-86.

Uebelhart, D., Thonar, E. J.-M. A., Pietryla, D. W., Williams, J. W., 1993. Elevation in urinary levels of pyridinium cross-links of collagen following chymopapin-induced degradation of articular cartilage in the rabbit knee provides evidence of metabolic changes in bone. Osteoarthritis Cartilage 1, 185-92.

Venn, M. F., Maroudas, A., 1977. Chemical composition and swelling of normal and osteoarthritic femoral head cartilage. I. Chemical composition. Ann Rheum Dis 36, 121-9.

Wang, C. C., Chahine, N. O., Hung, C. T., Ateshian, G. A., 2003. Optical determination of anisotropic material properties of bovine articular cartilage in compression. J Biomech 36(3), 339-53.

Williamson, A. K., Chen, A. C., Sah, R. L., 2001. Compressive properties and function-composition relationships of developing bovine articular cartilage. J Orthop Res 19, 1113-21.

Williamson, A. K., Chen, A. C., Masuda, K., Thonar, E. J.-M. A., Sah, R. L., 2003a. Tensile mechanical properties of bovine articular cartilage: variations with growth and relationships to collagen network components. J Orthop Res 21, 872-880.

Williamson, A. K., Masuda, K., Thonar, E. J.-M. A., Sah, R. L., 2003b. Growth of immature articular cartilage in vitro: correlated variation in tensile biomechanical and collagen network properties. Tissue Eng 9, 625-634.

Woessner, J. F., 1961. The determination of hydroxyproline in tissue and protein samples containing small proportions of this imino acid. Arch Biochem Biophys 93, 440-447.

Wong, M., Ponticiello, M., Kovanen, V., Jurvelin, J. S., 2000. Volumetric changes of articular cartilage during stress relaxation in unconfined compression. J Biomech 33(9), 1049-54.

Woo, S. L.-Y., Lubock, P., Gomez, M. A., Jemmott, G. F., Kuei, S. C., Akeson, W. H., 1979. Large deformation nonhomogeneous and directional properties of articular cartilage in uniaxial tension. J Biomech 12, 437-446.

TABLE AND FIGURE CAPTIONS

Table 1. Results (mean ± 1 S.D.) measured in CC (aggregate modulus H_A in MPa, permeability constants k_0 in 10^{-15} m^2/Pa·s, M), UCC (Young's modulus E in MPa, Poisson's ratios ν_{ij}) and TS (shear modulus μ in MPa) before (AX-D0, ML-D0) and after (AX-D14) growth. Subscripts 15, 30, 45 refer to strain levels of 15, 30, and 45%, respectively. Superscripts "d" and "g" indicate significant differences ($p<0.05$) due to direction and growth, respectively. Some AX-D14 properties were not measured because of considerable mechanical property degradation during growth.

Table 2. Results (mean ± 1 S.D.) for AP-D0 and AX-D14 groups. AP-D0 values are from specimens adjacent to the ML-D0 and AX-D0 specimens. AX-D14 values are from mechanically tested specimens after growth. % water (% W), COL (mg/g), GAG (mg/g), DNA (10^7 x cells/g), and PYR (nmol/g). Contents are normalized to tissue WW. Superscript "g" indicates a significant difference ($p<0.05$) due to growth.

Figure 1. Day zero (D0) specimen preparation included harvesting a full-thickness explant block from the medial ridge of the PFG, preparing three orthogonal slices, and punching one disc (diameter = 3.2 mm, height = 1 mm) from each slice at a 2mm mean depth. This protocol produces discs obtained from slices normal to local anatomical directions: medial-lateral (ML-D0), anterior-posterior (AP-D0), and axial (AX-D0).

Figure 2. In unconfined compression (A), a mirror and prisms project two lateral images of the specimen 90° apart to a digital camera. The light paths from the two cross sections travel horizontally to right angled prisms which project the light paths vertically upward to a flat mirror, which is angled at 45° to the horizontal and projects the light paths outward toward the digital camera. In torsional shear (B), porous platens apply rotation to the specimen.

Figure 3. Digital image of a cartilage explant (top) between two impermeable platens and calculated image obtained in MATLAB (bottom). The dark horizontal lines in the bottom figure represent the diameters that MATLAB computes by loading the original image and scanning through rows to find the positions where the change in pixel intensity is greatest.

Figure 4. CC modulus H_A and UCC modulus E results (mean ± 1 S.D.) before growth (D0). Data corresponds to cylindrical discs with axial directions aligned with ML and AX directions at strain levels of 15, 30, and 45%. H_A and E were independent of direction and strain level although values at 30% strain were lower than values at 15 and 45% strain.

Figure 5. UCC Poisson's ratios (ν_{ij}) results (mean ± 1 S.D.) before growth (D0). Data corresponds to cylindrical discs with axial directions aligned with ML and AX directions at a 30% strain level. * indicates a significant difference ($p<0.05$).

Figure 6. Relationship between shear modulus μ and normal stress σ at 0.5% shear strain and 10% offset compression strain before growth (D0). Data points correspond to cylindrical discs with axial directions aligned with the ML (△) and AX (□) directions. The y-intercept value of 0.113 MPa suggests a value for the infinitesimal shear modulus.

Figure 7. Relationships between mechanical properties and COL/PYR contents. CC modulus H_A, UCC modulus E, UCC Poisson's ratios ν_{31} and ν_{32} at 30% strain, permeability constants k_0 and M, and shear modulus μ at 10% offset compression strain. Data points correspond to cylindrical discs with axial directions aligned with the ML (△) and AX (□,■) directions before (D0; △,□) and after (D14; ■) growth. COL/PYR contents were measured from AX-D14 specimens and from AP-D0 specimens paired with the ML-D0 and AX-D0 specimens. Displayed regression lines and coefficients indicate significant correlations ($p<0.05$).

Figure 8. Relationships between mechanical properties and GAG/DNA contents. CC modulus H_A, UCC modulus E, UCC Poisson's ratios ν_{31} and ν_{32} at 30% strain, permeability constants k_0 and M, and shear modulus μ at 10% offset compression strain. Data points correspond to cylindrical discs with axial directions aligned with the ML (△) and AX (□,■) directions before (D0; △,□) and after (D14; ■) growth. GAG/DNA contents were measured from AX-D14 specimens and from AP-D0 specimens paired with the ML-D0 and AX-D0 specimens. Displayed regression lines and coefficients indicate significant correlations ($p<0.05$).

Table 1. Results (mean ± 1 S.D.) measured in CC (aggregate modulus H_A in MPa, permeability constants k_0 in 10^{-15} m^2/Pa·s, M), UCC (Young's modulus E in MPa, Poisson's ratios ν_{ij}) and TS (shear modulus μ in MPa) before (AX-D0, ML-D0) and after (AX-D14) growth. Subscripts 15, 30, 45 refer to strain levels of 15, 30, and 45%, respectively. Superscripts "d" and "g" indicate significant differences ($p<0.05$) due to direction and growth, respectively. Some AX-D14 properties were not measured because of considerable mechanical property degradation during growth.

	AX - D0	**ML - D0**	**AX - D14**
$H_{A,15}$	0.564 ± 0.178^{g}	0.532 ± 0.259	0.062 ± 0.026^{g}
$H_{A,30}$	0.510 ± 0.135^{g}	0.513 ± 0.195	0.071 ± 0.027^{g}
$H_{A,45}$	0.610 ± 0.159	0.613 ± 0.239	not measured
k_0	1.547 ± 2.254	0.653 ± 0.384	1.272 ± 0.852
M	6.069 ± 2.394	5.180 ± 1.614	6.014 ± 1.435
E_{15}	0.606 ± 0.210^{g}	0.564 ± 0.256	0.022 ± 0.024^{g}
E_{30}	0.528 ± 0.177^{g}	0.471 ± 0.204	0.022 ± 0.022^{g}
E_{45}	0.634 ± 0.224	0.558 ± 0.242	not measured
$\nu_{12,15}$	N/A	0.143 ± 0.063	N/A
$\nu_{12,30}$	N/A	0.142 ± 0.062	N/A
$\nu_{12,45}$	N/A	0.150 ± 0.085	N/A
$\nu_{13,15}$	N/A	0.219 ± 0.150	N/A
$\nu_{13,30}$	N/A	0.232 ± 0.133^{d}	N/A
$\nu_{13,45}$	N/A	0.253 ± 0.148^{d}	N/A
$\nu_{31,15}$	0.138 ± 0.081^{g}	N/A	0.435 ± 0.213^{g}
$\nu_{31,30}$	0.141 ± 0.080^{g}	N/A	0.458 ± 0.203^{g}
$\nu_{31,45}$	0.156 ± 0.083	N/A	not measured
$\nu_{32,15}$	0.127 ± 0.063^{g}	N/A	0.371 ± 0.185^{g}
$\nu_{32,30}$	0.119 ± 0.039^{d,g}	N/A	0.440 ± 0.139^{g}
$\nu_{32,45}$	0.125 ± 0.049^{d}	N/A	not measured
μ	0.918 ± 0.409	0.723 ± 0.422	not measured

Table 2. Results (mean ± 1 S.D.) for AP-D0 and AX-D14 groups. AP-D0 values are from specimens adjacent to the ML-D0 and AX-D0 specimens. AX-D14 values are from mechanically tested specimens after growth. % water (% W), COL (mg/g), GAG (mg/g), DNA (10^7 x cells/g), and PYR (nmol/g). Contents are normalized to tissue WW. Superscript "g" indicates a significant difference ($p<0.05$) due to growth.

	AP- D0	**AX-D14**
% W	86.0 ± 1.4	86.2 ± 7.8
COL	100.0 ± 18.3^{g}	46.6 ± 23.9^{g}
GAG	47.6 ± 8.5^{g}	30.1 ± 16.4^{g}
DNA	9.4 ± 1.9^{g}	4.7 ± 2.1^{g}
PYR	95.5 ± 29.4^{g}	45.5 ± 12.3^{g}

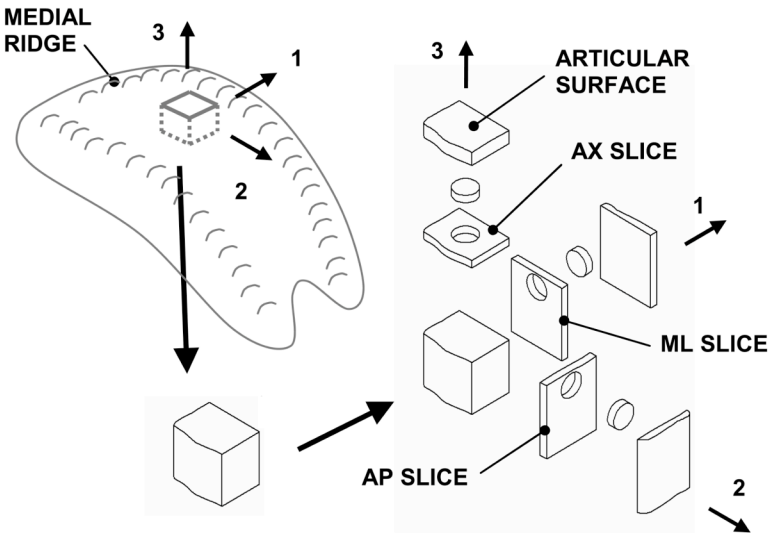

Figure 1. Day zero (D0) specimen preparation included harvesting a full-thickness explant block from the medial ridge of the PFG, preparing three orthogonal slices, and punching one disc (diameter = 3.2 mm, height = 1 mm) from each slice at a 2mm mean depth. This protocol produces discs obtained from slices normal to local anatomical directions: medial-lateral (ML-D0), anterior-posterior (AP-D0), and axial (AX-D0).

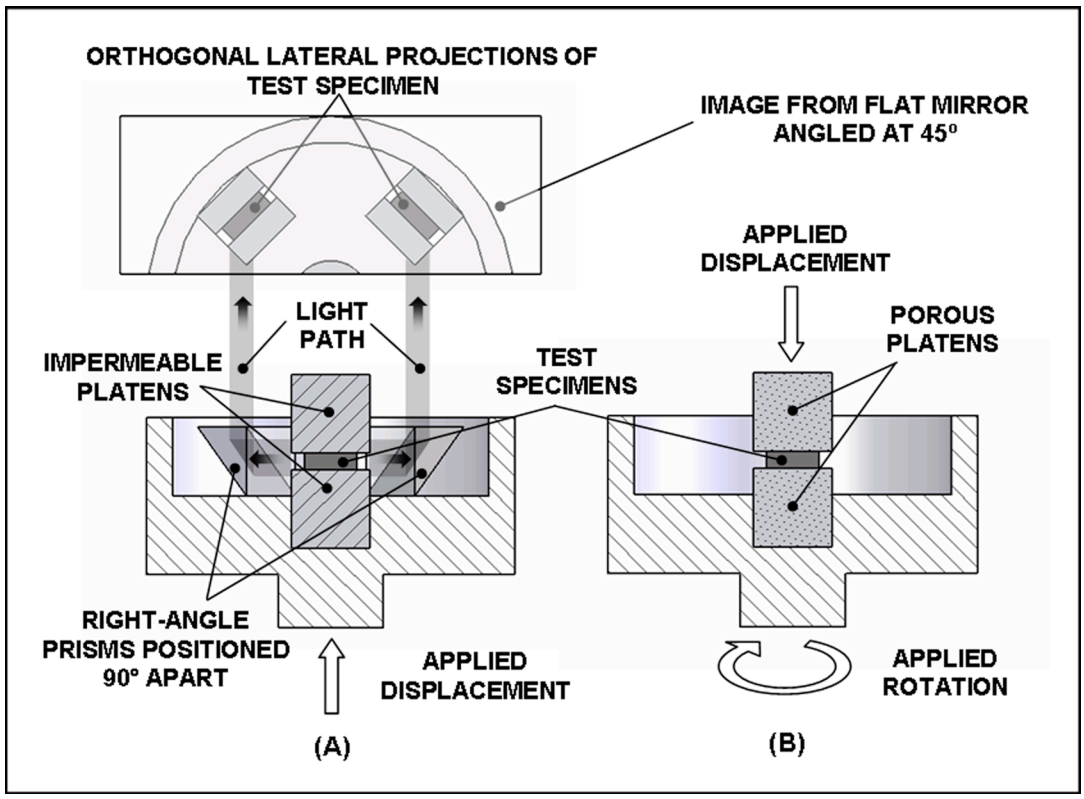

Figure 2. In unconfined compression (A), a mirror and prisms project two lateral images of the specimen 90° apart to a digital camera. The light paths from the two cross sections travel horizontally to right angled prisms which project the light paths vertically upward to a flat mirror, which is angled at 45° to the horizontal and projects the light paths outward toward the digital camera. In torsional shear (B), porous platens apply rotation to the specimen.

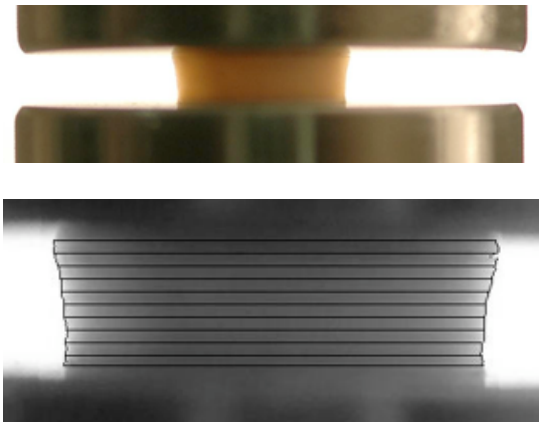

Figure 3. Digital image of a cartilage explant (top) between two impermeable platens and calculated image obtained in MATLAB (bottom). The dark horizontal lines in the bottom figure represent the diameters that MATLAB computes by loading the original image and scanning through rows to find the positions where the change in pixel intensity is greatest.

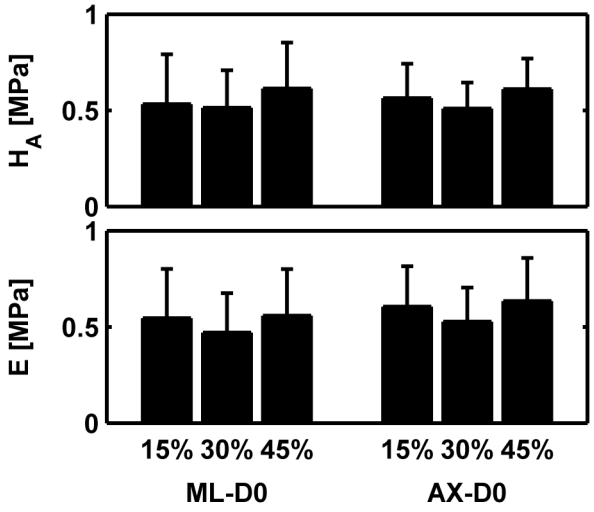

Figure 4. CC modulus H_A and UCC modulus E results (mean ± 1 S.D.) before growth (D0). Data corresponds to cylindrical discs with axial directions aligned with ML and AX directions at strain levels of 15, 30, and 45%. H_A and E were independent of direction and strain level although values at 30% strain were lower than values at 15 and 45% strain.

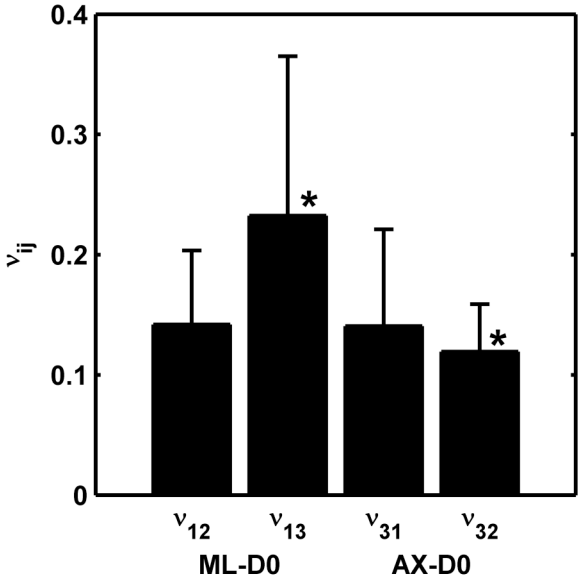

Figure 5. UCC Poisson's ratios (ν_{ij}) results (mean ± 1 S.D.) before growth (D0). Data corresponds to cylindrical discs with axial directions aligned with ML and AX directions at a 30% strain level. * indicates a significant difference ($p<0.05$).

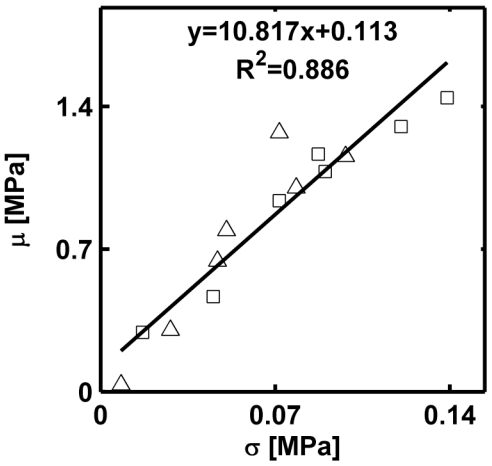

Figure 6. Relationship between shear modulus μ and normal stress σ at 0.5% shear strain and 10% offset compression strain before growth (D0). Data points correspond to cylindrical discs with axial directions aligned with the ML (△) and AX (□) directions. The y-intercept value of 0.113 MPa suggests a value for the infinitesimal shear modulus.

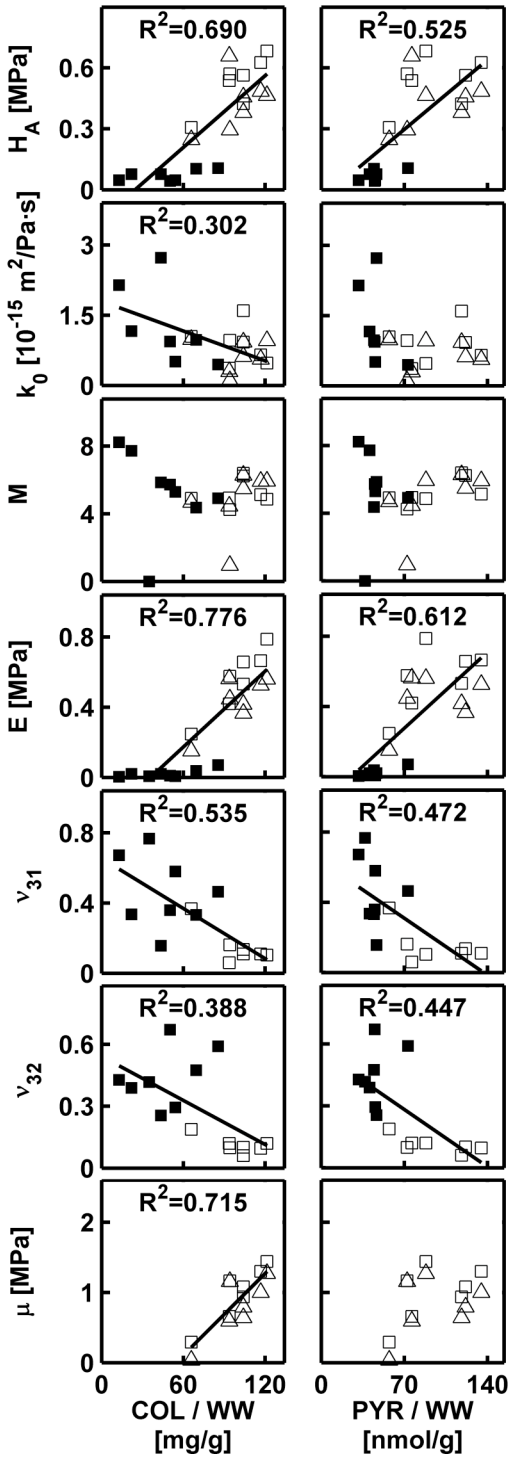

Figure 7. Relationships between mechanical properties and COL/PYR contents. CC modulus H_A, UCC modulus E, UCC Poisson's ratios ν_{31} and ν_{32} at 30% strain, permeability constants k_0 and M, and shear modulus μ at 10% offset compression strain. Data points correspond to cylindrical discs with axial directions aligned with the ML (△) and AX (□,■) directions before (D0; △,□) and after (D14; ■) growth. COL/PYR contents were measured from AX-D14 specimens and from AP-D0 specimens paired with the ML-D0 and AX-D0 specimens. Displayed regression lines and coefficients indicate significant correlations ($p<0.05$).

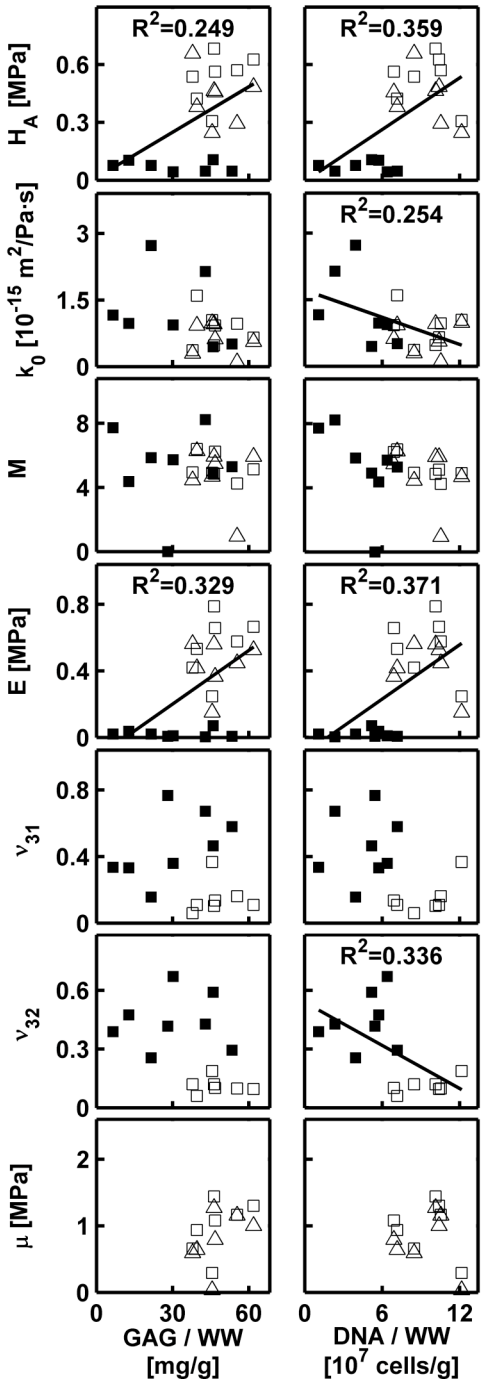

Figure 8. Relationships between mechanical properties and GAG/DNA contents. CC modulus H_A, UCC modulus E, UCC Poisson's ratios ν_{31} and ν_{32} at 30% strain, permeability constants k_0 and M, and shear modulus μ at 10% offset compression strain. Data points correspond to cylindrical discs with axial directions aligned with the ML (△) and AX (□,■) directions before (D0; △,□) and after (D14; ■) growth. GAG/DNA contents were measured from AX-D14 specimens and from AP-D0 specimens paired with the ML-D0 and AX-D0 specimens. Displayed regression lines and coefficients indicate significant correlations ($p<0.05$).